



Dual luminescent charge transfer probe for quantitative detection of serum albumin in aqueous samples

Rajib Choudhury*, Benjamin Quattlebaum, Charles Conkin, Siddhi Rajeshbhai Patel, Kallie Mendenhall

Department of Physical Sciences, Arkansas Tech University, Russellville, AR 72801, United States

ARTICLE INFO

Article history:

Received 6 January 2020

Received in revised form 14 March 2020

Accepted 24 March 2020

Available online 24 March 2020

Keywords:

Dual emission probe

Selective protein recognition

Near infrared emission

Human serum albumin

Microalbuminuria

ABSTRACT

In diagnostic medicine serum albumin is considered as an important biomarker for assessment of cardiovascular functions and diagnosis of renal diseases. Herein, we report a novel donor- π - π -acceptor fluorophore for selective detection of serum albumin in urine samples. In our design, a phenolic donor was conjugated with a tricyanofuran (TCF) acceptor through a dimethine bridge via a simple condensation reaction. The stereoelectronic effects of the incorporated methoxy ($-\text{OCH}_3$) groups and the TCF moiety—in conjunction with the extended π -electron conjugation—led to dual red and NIR-I absorption/emission in water. Moreover, due to superior electron transfer between a phenolate donor and the TCF acceptor and the subsequent energy decay from the charge transfer states, the fluorophore displayed negligible fluorescence emission in water and other polar solvents. Consequently, we have been able to utilize the fluorophore for quantitative estimation of serum albumin both in the red (<700 nm) and NIR-I (700–900 nm) regions of the electromagnetic spectrum with excellent reproducibility. The fluorophore selectively recognized human serum albumin over other proteins and enzymes with a limit of detection of 10 mg/L and 20 mg/L in simulated urine samples at red and NIR-I emission window of the spectrum, respectively. By molecular docking analysis and experimental displacement assays, we have shown that the selective response of the fluorophore toward human serum albumin is due to tighter supramolecular complexation between the fluorophore and the protein at subdomain IB, and the origin of the NIR-I (780 nm) emission was attributed to a twisted conformer of phenolate- π - π -TCF system in aqueous solution. These findings indicate that the fluorophore could be utilized for quantitative detection of human serum albumin in urine samples for clinical diagnosis of albuminuria.

© 2020 Elsevier B.V. All rights reserved.

1. Introduction

Serum albumin is a major protein component of blood plasma [1–3]. It maintains osmotic blood pressure and facilitates transport of drugs, fatty acids, and other metabolites through blood stream [2]. Normally, in healthy individuals serum albumin is excreted with urine below 20 mg/L [2,4]. However, this amount might increase due to complicated health conditions. For instance, HSA level between 20 and 200 mg/L in urine—a medical term is known as microalbuminuria—has been linked to the risk of cardiovascular disease and early stages of kidney damage [2,5,6]. Amount >200 mg/L is diagnosed as macroalbuminuria—a condition which indicates advanced stages of kidney damage [2,5,6]. In other words, an elevated level of albumin in urine could indicate that the kidneys are no longer functioning properly. Therefore, quantitative detection of serum albumin in biological samples, such as in urine, is of

significant importance for early diagnosis of renal damage and cardiovascular disease.

Quantitative estimation of serum albumin by bio-analytical techniques has been reported in literature [7–14]. Some common examples are kinetic method, immunoelectrophoresis, spectrophotometric technique, immunoturbidimetry, enzyme-linked immunosorbent assay (ELISA), and radioimmunoassay [7–14]. Though some of these techniques are currently in use, they are not free from intrinsic drawbacks, such as, poor sensitivity and selectivity, extensive sample preparation method, requirement for other biomolecules and enzymes for assay preparation, and high cost associated with the specialized reagents and apparatus [14,15]. Therefore, fluorescence based detection and monitoring of serum albumin has attracted much attentions recently, mainly because of high sensitivity and simple operation methodology associated with a fluorimetric technique [16–22]. However, successful application of fluorescence based technique is limited due to lack of suitable fluorophores—a suitable fluorophore interacts and fluoresces only in presence of a target analyte. Recently, a handful of small molecule fluorophores have been reported for quantitative estimation of

* Corresponding author.

E-mail address: rchoudhury@atu.edu (R. Choudhury).

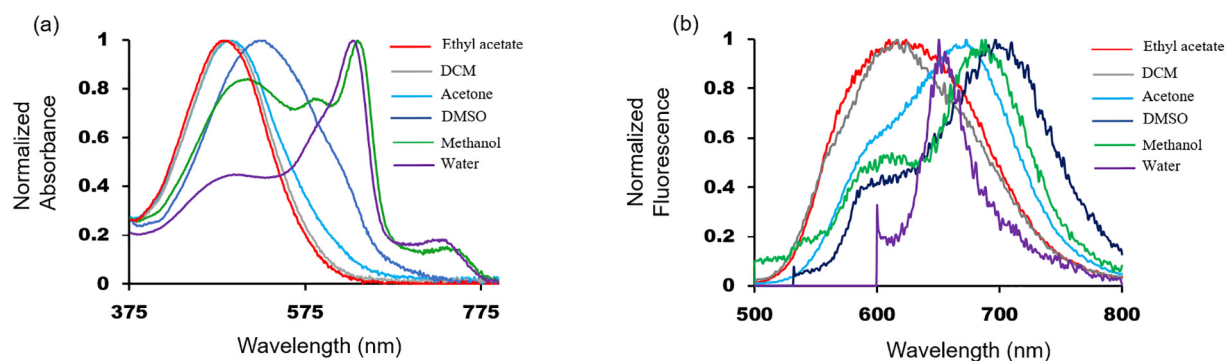


Fig. 1. (a) Absorption spectra of probe **1** in various solvents. $[1] = 1.0 \times 10^{-5}$ M. Aqueous solution contains 1% DMSO. (b) Fluorescence spectra of probe **1** in various solvents. $[1] = 1.0 \times 10^{-5}$ M. Aqueous solution contains 1% DMSO. For emission spectra, all the samples were excited at the absorption maxima, except for in methanol solution ($\lambda_{\text{ex}} = 485$ nm in methanol).

serum albumin in buffer as well as urine samples, but they encounter some limitations such as poor analyte selectivity, low aqueous solubility, low sensitivity, extensive preparation method, and high background fluorescence [9,18,19,23–26].

Herein, we have reported development of a new phenol based donor- π - π -acceptor probe, which displayed selective fluorescence response with human serum albumin in the red (665 nm) and NIR-I (780 nm) region of the electromagnetic spectrum [27]. The fluorophore exhibited sufficient aqueous solubility to hinder any aggregate formation in the test samples. Moreover, it remained ionized within a broad pH range—including at neutral pH—due to stereo-electronic properties of the incorporated methoxy ($-\text{OCH}_3$) and tricyanofuran (TCF) groups (Fig. 2c) [22,28]. In aqueous solution the ionized form populated the charge transfer (CT) states considerably. Therefore, significant amount of excited state energy was lost via competing non-radiative decays [29]. As a result, the background fluorescence of the probe was very low. The quenched emissions were then recovered upon complexation of the fluorophore within the protein's subdomain, resulting 10 mg/L and 20 mg/L limit of detection (LOD) in simulated urine solutions in the red and NIR-I region of the spectrum, respectively. The fluorophore selectively responded to human serum albumin (HSA) over homologue bovine serum albumin (BSA) and other proteins and enzymes with rapid enhancement of the fluorescence emission in both aqueous buffer and simulated urine samples. By employing fluorescence titrations, displacement assays, and molecular docking studies the underlying mechanism of the high selectivity was examined, and it was attributed to the site-specific supramolecular complexation of the fluorophore with HSA. Moreover, high sensitivity, superior selectivity, and dual emission window resulted quantitative detection of serum albumin in human urine samples, both in the red and NIR-I widow.

2. Results and discussion

Probe **1** was synthesized in two steps as shown in Scheme S1 (electronic supplementary information) [20]. First, to obtain the TCF acceptor (**C**), 3-hydroxy-3-methylbutan-2-one was refluxed with malononitrile and sodium ethoxide under N_2 atmosphere. TCF intermediate was then coupled with 3-(4-hydroxy-3,5-dimethoxyphenyl)acrylaldehyde via Knoevenagel condensation in presence of a weak base to yield the target probe (**1**). The probe was purified by silica gel chromatography and characterized by IR, NMR, and elemental analysis (Figs. S1 and S2, electronic supplementary information). In the IR spectrum, presence of a sharp signal at ~ 2200 cm^{-1} and a broad signal at ~ 3320 cm^{-1} indicate nitrile and phenolic functional group, respectively (Fig. S2). In the ^1H NMR spectrum, signal at 3.82 ppm confirmed presence of $-\text{OCH}_3$ groups attached to a phenyl moiety [22]. Moreover, its similar integral ratio with signal at 1.76 ppm on the TCF moiety suggests a successful condensation reaction. Additionally, the broad downfield shifted signal

at ~ 9.65 ppm in DMSO confirmed the presence of a phenolic $-\text{OH}$ group on **1** (Fig. S2). Selectivity to all-*trans* isomer for the condensation reaction was very high, at least within the limits of the NMR timescale. Presence of *trans* hydrogens was confirmed from the large coupling constants ($J = 16$ Hz) [30].

The absorption and emission maxima of **1** displayed a noticeable dependence on the solvent polarity. As shown in Fig. 1a, as the polarity of the solvent increased, the $\lambda_{\text{max}}^{\text{abs}}$ bathochromically shifted. In polar protic solvents, such as water and methanol, the absorption spectra were more structured and extended in the NIR-I region. Similarly, the fluorescence spectra showed positive solvent dependency; ~ 80 nm bathochromic shift—along with reduced intensity—was recorded when solvent was switched from ethyl acetate to dimethyl sulfoxide. In general, the fluorescence intensities in polar solvents were lower than that of the non-polar solvents, in agreement with the formation of the solvent stabilized charge transfer states [29,31]. Also, the quantum yield of **1** was calculated in three different solvents with respect to a reference dye and it was found to be 0.001 in DMSO, 0.003 in methanol, and 0.012 in acetone.

Phenol is moderately acidic in water ($\text{pK}_a \approx 10$). However, its pK_a can be lowered by incorporating electron withdrawing group(s) on the benzene ring [32]. Interestingly, **1** remains predominantly in the deprotonated form in pH 7.4 buffer solution ($\lambda_{\text{max}}^{\text{abs}} = 630$ nm; $\epsilon = 28,480$ $\text{Lmol}^{-1} \text{cm}^{-1}$, Fig. 2a). The signal at 480 nm was attributed to the neutral form which gradually decreased upon increasing the pH from 4.0–6.0–7.4–9.0, passing through an isobestic point at 540 nm. It completely disappeared at $\sim \text{pH}$ 9.0, indicating presence of highest fraction of deprotonated form (Fig. 2c, ionic form I); the extinction coefficient at λ_{max} was greater at pH 9.0 and 10.0 than pH 7.4. Fluorescence of **1** was also recorded in different buffer solutions (Fig. 2b). When **1** was excited at 480 nm, broad structured emission (range: 550–750 nm; Stokes' shift 135 nm) was observed. On the other hand, narrow, low-intensity signals were observed upon excitation ($\lambda_{\text{ex}} = 630$ nm) of the deprotonated forms, displaying a small Stokes' shift (~ 25 nm).

Probe **1** exhibited an absorption band at 740 nm ($\epsilon = 3790$ $\text{Lmol}^{-1} \text{cm}^{-1}$) in pH 7.4 buffer solution (Fig. 2a). The intensity of the signal increased at higher pH ($\epsilon = 19,960$ $\text{Lmol}^{-1} \text{cm}^{-1}$ at pH 9.0; $\epsilon = 20,470$ $\text{Lmol}^{-1} \text{cm}^{-1}$ at pH 10.0), indicating existence of another solvent stabilized form of **1** in water, and its amount increases as the basicity of the solution increases. Presumably, this is a twisted conformer, such as a cisoid conformer, of **1** which originates from the rotations of the bonds in the dimethine bridge. Moreover, the 110 nm bathochromic shift appears only when there is a significant amount of deprotonated form (ionic form I) present in the solution; no absorption beyond 630 nm was detected in pH 6.0 buffer solution, indicating strong donor-acceptor charge transfer is required in the ground state for population of this twisted conformer [33]. In our previous studies, no such

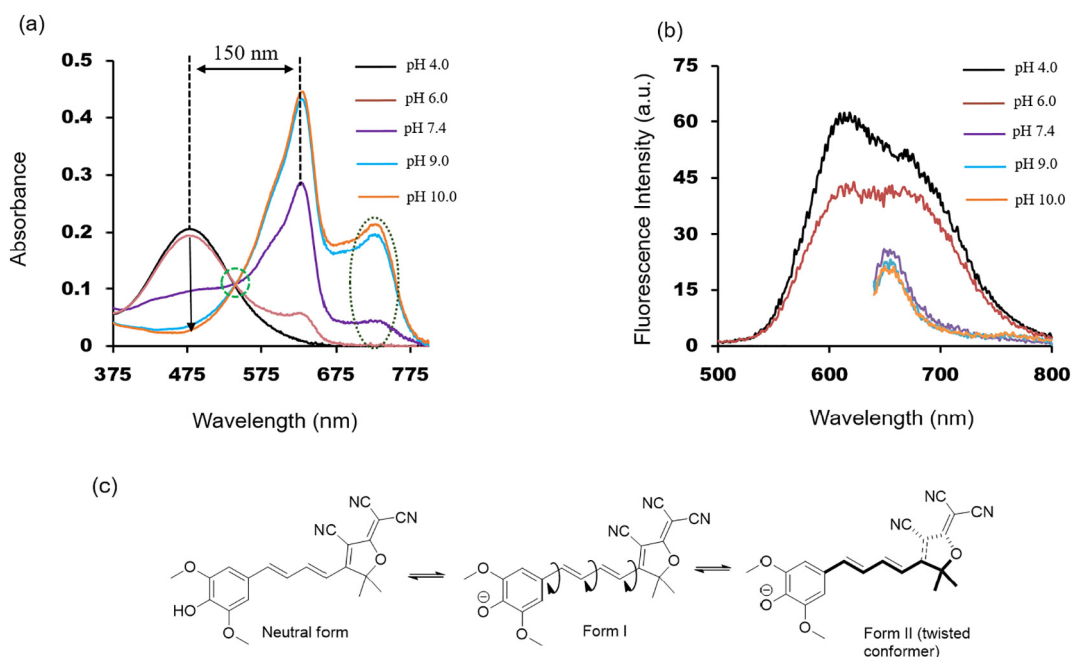


Fig. 2. (a) Absorption spectra of **1** in water at different pH values. (b) Fluorescence spectra of **1** in water at different pH values. All the aqueous solutions contain 1% DMSO. For emission spectra, all the samples were excited at the absorption maxima. (c) Protonated, deprotonated, and probable twisted conformer of **1** in water. [**1**] = 1.0×10^{-5} M. Green circle indicates the isobestic point. Dotted ellipse shows absorption centered at 740 nm in higher pH solutions.

near infrared absorption was recorded with one alkenyl conjugated phenolate- $O^{(-)}$ - π -acceptor fluorophore, suggesting that this is unique for a phenolate- $O^{(-)}$ -dimethine-acceptor system [22].

Phenolate- $O^{(-)}$ is a better electron donating group than phenol-OH [22,32]. To find a correlation between the donor strength and the optical properties **1**, semi-empirical calculations (ZINDO/1) were performed on HyperChem suite in gas phase, and the HOMO/LUMO were plotted for

both neutral and deprotonated form (ionic form I). As shown in Fig. 3a, the π -electrons on the HOMO of neutral **1** was delocalized on the π -conjugated framework, but the LUMO was positioned near the acceptor side. When the phenol-OH was deprotonated, the HOMO was mainly centered at the phenolate site, and for the LUMO the larger lobes were observed on the acceptor unit. In fact, it is the large destabilization of the HOMO of the phenolate- $O^{(-)}$ reduces the overall HOMO/

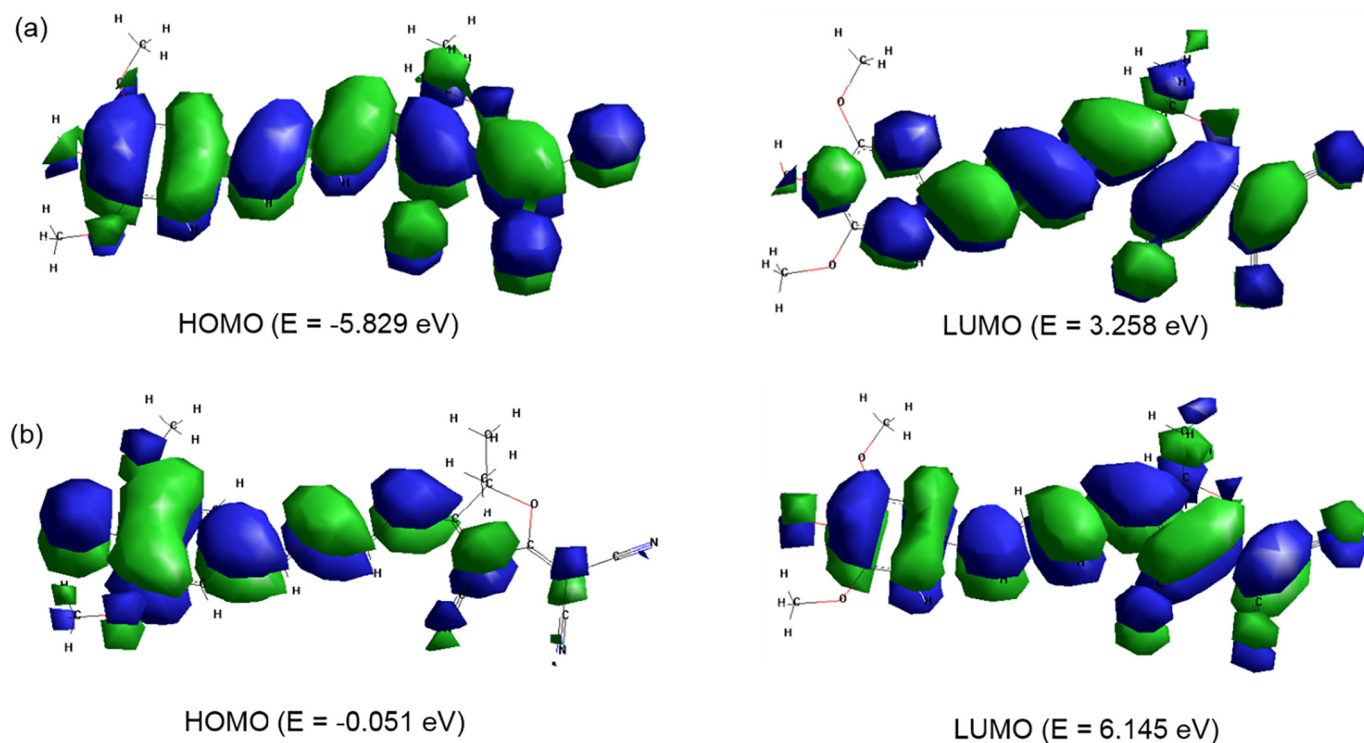


Fig. 3. (a) Molecular orbital plots (HOMO and LUMO) and the corresponding energies of the neutral form (Fig. 2c) in the ground state. (b) Molecular orbital plots (HOMO and LUMO) and the corresponding energies of the ionic form I (Fig. 2c) in the ground state.

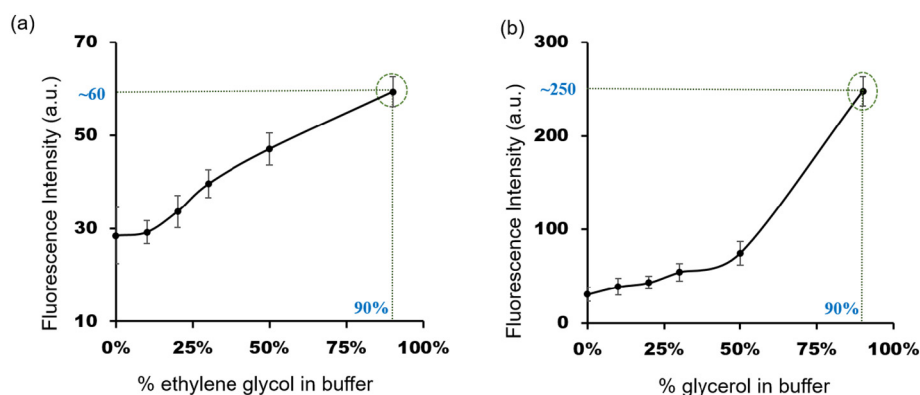


Fig. 4. (a) Fluorescence spectra of **1** (10 μ M) in different ratios of buffer (pH = 7.4)-ethylene glycol mixtures, $\lambda_{\text{ex}} = 630$ nm. (b) Fluorescence spectra of **1** (10 μ M) in different ratios of buffer (pH = 7.4)-glycerol mixtures, $\lambda_{\text{ex}} = 630$ nm.

LUMO gap, most likely responsible for the large shift of λ_{max} (150 nm) in the absorption spectrum (Fig. 2a).

In polar solvents—as well as in basic buffer solutions—**1** exhibits low fluorescence intensity, suggesting energy loss from the excited states via non-radiative pathways (Figs. 1b and 2b). Fig. 4 shows effect of solution viscosity on the fluorescence emission of **1** ($\lambda_{\text{ex}} = 630$ nm). Ethylene glycol and glycerol are viscous liquids (viscosity of ethylene glycol 35.7 and glycerol 950 cP at 25 $^{\circ}$ C, respectively) [29,31,34]. Upon increasing the glycerol amount in a water-glycerol mixture of **1**, a systematic fluorescence enhancement was observed (Fig. 4b). Similar results were obtained in ethylene glycol-water mixtures (Fig. 4a). Two fold and four fold fluorescence enhancement was recorded in 9:1 water-ethylene glycol and water-glycerol mixture, respectively, suggesting restriction of conformational freedom of the rotatable bonds [29].

Conformational change about the dimethine chain connecting the phenolate donor and the TCF acceptor can be prevented in a highly viscous microenvironment. Consequently, we investigated the optical properties of **1** in presence of human serum albumin in aqueous buffer

solution. Upon addition of one equivalent of HSA into a solution of **1** (10 μ M; pH 7.4 buffer), the absorption maxima bathochromically (~ 18 nm) and hyperchromically shifted, suggesting a ground state complex formation (Fig. S3, electronic supplementary information) [35]. The fluorescence emission increased fifteen fold (Q.Y. of **1** in buffer was 0.01 and in presence of one equivalent HSA was 0.10) when **1** was excited at 630 nm in presence of one equivalent of HSA (excitation spectra Fig. S4a, electronic supplementary information). Similarly, upon excitation at 740 nm, fifteen fold increase in emission at ~ 780 nm was recorded under identical experimental conditions (Fig. 5b, excitation spectra Fig. S4b, electronic supplementary information). A concentration dependent study in simulated urine samples revealed a linear relationship between the emission and the HSA up to 500 mg/L for the red emission ($\lambda_{\text{max}}^{\text{em}} \sim 665$ nm) and 300 mg/L ($\lambda_{\text{max}}^{\text{em}} \sim 780$ nm) for the NIR emission. From these concentration dependent fluorescence data the limit of detections (LOD) were calculated ($\text{LOD} = 3\sigma/\text{slope}$), and they were found to be 10 mg/L and 20 mg/L, respectively (Fig. 5c for the red emission and Fig. 5d for the NIR-I emission) [36]. (Table S1,

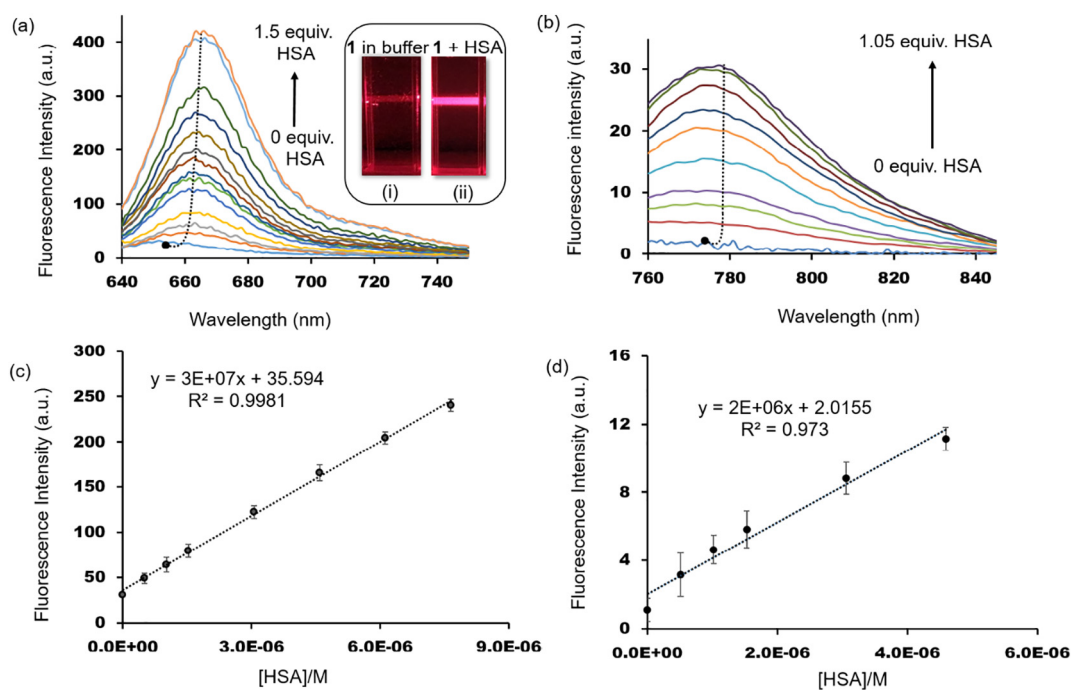


Fig. 5. (a) Plot of emission ($\lambda_{\text{ex}} = 630$ nm) of probe **1** in the presence of HSA. Inset: Showing fluorescence of **1** in absence (i) and presence (ii) of one equivalent of HSA when excited with a laser (source 630 nm). (b) Plot of emission ($\lambda_{\text{ex}} = 740$ nm) of probe **1** in the presence of HSA. (c) Linear relationship between the emission maxima of **1** ($\lambda_{\text{em}}^{\text{max}} \sim 665$ nm) and the amount of HSA in simulated urine. (d) Linear relationship between the emission maxima of **1** ($\lambda_{\text{em}}^{\text{max}} \sim 780$ nm) and the amount of HSA in simulated urine.

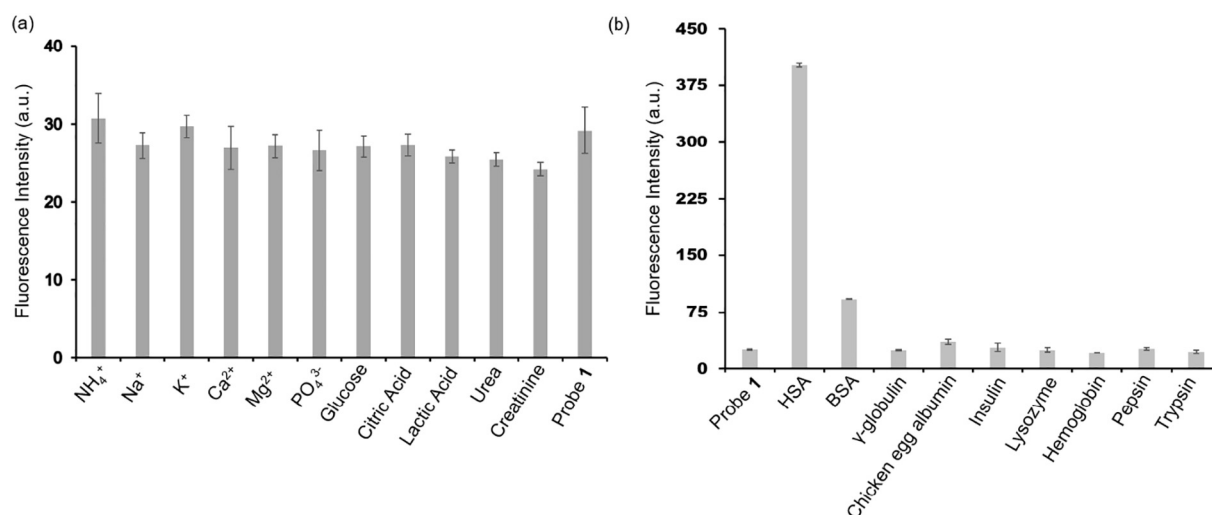


Fig. 6. (a) Fluorescence emission of **1** (10 μM) in presence of various ions and bio-analytes, $\lambda_{\text{ex}} = 630$ nm. (b) Fluorescence emission of **1** (10 μM) in presence of HSA and other biomacromolecules in phosphate buffer (pH = 7.4), $\lambda_{\text{ex}} = 630$ nm.

electronic supplementary information) These wide detection ranges make **1** a promising probe for estimation of HSA in normal and microalbuminuria conditions. Moreover, as shown in Fig. S5 (electronic supplementary information), the emission did not change under normal laboratory lights. The emission intensity almost immediately enhanced upon addition of HSA, and it was constant over an extended period of time.

Next, the interfering effect of ionic species and bio-analytes—commonly found in urine— was investigated. No significant change in fluorescence emission ($\lambda_{\text{ex}} = 630$ nm) of **1** (10 μM) was observed in presence of external species, up to a concentration as high as 200 micro-molars (Fig. 6a). Additionally, the selective response property was studied by measuring the fluorescence emission of **1** ($\lambda_{\text{em}} = 665$ nm, $\lambda_{\text{ex}} = 630$ nm) in the presence of several proteins and enzymes such as BSA (a homologue HSA), γ -globulin (antibody isotype), chicken egg albumin, insulin, lysozyme, hemoglobin, pepsin, and trypsin (Fig. 6b). Our probe selectively recognized HSA. Though slight fluorescence enhancement (~3 fold) was observed in presence of BSA; its presence is unlikely in the urine samples. Other biomolecules, including γ -globulin, had no effect on the fluorescence of **1** (Fig. 6b). Similar selective recognition was also observed with the NIR-I emission wavelength at ~780 nm (Fig. S6, electronic supplementary information, $\lambda_{\text{ex}} = 740$ nm). To test the stability and performance of **1**, three real human urine samples were spiked with serum albumin and fluorescence intensities were measured at both emission wavelengths. The measured fluorescence intensities were fitted to the standard curve and the amounts

of serum albumin were calculated from the linear relationship between fluorescence intensity and the concentration of albumin. The calculated amount obtained from the standard curve was found to be very similar to the added amount of HSA (Table S2, electronic supplementary information). Moreover, ~16-fold fluorescence enhancement was recorded in human blood serum in presence of 10 μM of **1**.

To probe the high selectivity and turn-on sensing mechanism of **1**, ligand competitive experiments with three site specific compounds (warfarin, domain IIA marker; salicylic acid, site marker for subdomains IB and IIA; ibuprofen, site IIIA marker) were performed [37,38]. The emission at ~665 nm ($\lambda_{\text{ex}} = 630$ nm) was monitored for all the experiments. Addition of incremental amount of warfarin (10, 20, 30, 40 and 50 μM) in the mixtures of **1**@HSA resulted increase in fluorescence emission (Fig. 7a). An overall ~50% increase in fluorescence was recorded. Whereas, addition of salicylic acid ($K_a = 6.0 \times 10^4 \text{ M}^{-1}$) decreased the fluorescence up to ~70% (Fig. 7a), and ibuprofen did not change the fluorescence of **1**@HSA (Fig. S7a, electronic supplementary information). Addition of even excess (12 equiv.) did not show any effect on the fluorescence of **1**@HSA complex. More importantly, myristic acid (a site IB binder) reduced the fluorescence emission of **1** by ~85% of the original value (Fig. S7b, electronic supplementary information). Separate control experiments with all the site specific markers have confirmed absence of any quenching for **1** in buffer solutions.

As probe **1** is non-fluorescent in aqueous buffer, an increase in signal intensity upon addition of warfarin might suggest two events: (1) warfarin displaces **1** from the binding pocket, and (2) **1** translates into other

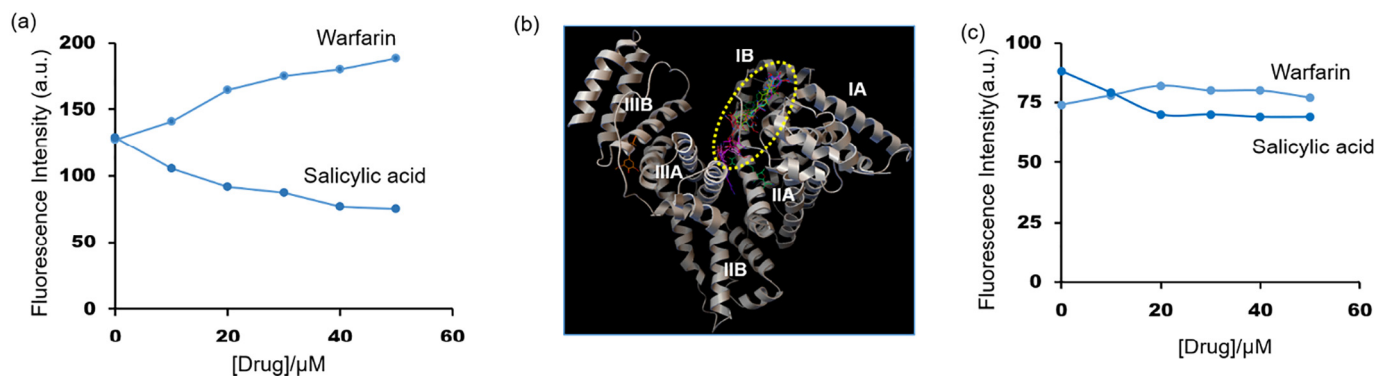


Fig. 7. (a) The change in fluorescence intensity at 665 nm ($\lambda_{\text{ex}} = 630$ nm) upon addition of increasing concentrations of site specific compounds warfarin and salicylic acid to the complexes of **1** (5 μM) and HSA (333 mg/L). (b) Docking conformation of **1**@HSA complex showing predominant bindings at site IB. (c) The change in fluorescence intensity at 665 nm ($\lambda_{\text{ex}} = 630$ nm) upon addition of increasing concentrations of site specific compounds warfarin and salicylic acid to the complexes of **1** (5 μM) and BSA (333 mg/L).

binding site(s) of the protein when a competitive binder (warfarin, $K_a = 3.4 \times 10^4 \text{ M}^{-1}$) is present in the solution. However, with salicylic acid an opposite effect was observed. Upon addition of increasing amount of salicylic acid (10, 20, 30, 40 and 50 μM), the fluorescence intensity gradually decreased to an overall 70% less than the original, indicating effective displacement of **1** from the HSA. Salicylic acid binds at both subdomain IB and IIA [39]. Therefore, the effective displacement by salicylic acid indicates that **1** binds predominantly at IB or between IB and IIA; in the latter scenario, it would be displaced and migrated into the subdomain IB in presence of a site IIA binder—such as warfarin. The fluorescence enhancement in presence of warfarin explains that phenomenon, as discussed earlier. In summary, based on these displacement experiments, we conclude that **1** predominantly binds within the IB subdomain of HSA.

To obtain a more realistic view of the binding site within HSA, molecular dockings were performed with AutoDock Vina program [40]. Total three blind dockings were performed, and in each docking the search space included the entire surface of the protein. The binding energy for each pose was negative, suggesting spontaneous, energetically favorable binding process. As shown in Fig. 7b, **1** was mainly (93% of the total 27 conformers) bound at site IB, thus corroborating with the experiments.

On the other hand, the site specific binders exhibited minimal displacement when titrated against **1**@BSA complex (Fig. 7c), as revealed by the minimal change of fluorescence emission. For warfarin 4% increase and for salicylic acid 21% decrease was recorded, respectively (Fig. 7c). As anticipated, insignificant change in intensity was observed when a 1:1 complex of **1**@BSA was titrated with ibuprofen. All these displacement assays suggest that **1** does not bind in the common drug binding sites of BSA. Therefore, to obtain a visual perspective of the complexation site, three blind molecular dockings were performed with BSA. As shown in Fig. S8 (electronic supplementary information), **1** predominantly binds between site IB and IIIA (60% of the total 27 conformers), which is in accordance with the displacement experiments, and only 11% of the conformers were located at site IB.

From the experimental and molecular modelling results the selective response of **1** toward HSA can be attributed to its site-specific complexation with HSA. The calculated average binding energy obtained from the molecular dockings (-8.8 kcal/mol)—as well as the experimentally determined association constant (Benesi-Hildebrand plot; $K_a = 1.4 \times 10^5 \text{ M}^{-1}$; Fig. S9, electronic supplementary information)—suggest a strong supramolecular complex between **1** and HSA [18,41]. Site I in HSA comprises four helix bundles located in subdomain IB. This site is water accessible, however, it is more hydrophobic than the site I of BSA [42]. The hydrophobic residue Phe 122 and two other hydrophobic residues res 120 and res 126 are located on a small surface exposed helix. At site IB, the hydrophobic as well as other non-covalent interactions, such as polar interaction with lysine 137, rigidify the fluorophore, which could make it more emissive in the bound state (Fig. S10a, b, and d in electronic supplementary information) [18–22]. On the other hand, poor interactions (average binding energy = -7.6 kcal/mol obtained from the molecular dockings) of **1** with BSA at a non-specific site (between domain I and III, Fig. S8) most likely results minimal fluorescence enhancement (Figs. S10c, d, and S11, electronic supplementary information). In case of BSA, **1** was predominately found at the intersection between IB and III (Figs. S8 and S10d in electronic supplementary information). This intersection is solvent accessible and the amino acid sequence differs from HSA in several analogous helix regions [42]. For example, between HSA and BSA at analogous residues 189 and 190, HSA is very hydrophilic whereas BSA is strongly hydrophobic. The composition of amino acid sequence between 455 and 457 at site III in BSA also differs from HSA. But, both are considered as very hydrophobic. Moreover, at the binding site of BSA no polar interactions between **1** and residues were found from the molecular docking analysis. These docking results demonstrate that **1** selectively binds at site IB which results in the difference in fluorescence response from BSA.

Furthermore, in highly viscous glycerol, the emission intensity at 780 nm increases dramatically. An eight fold enhancement was recorded with 90% glycerol in phosphate buffer (Fig. S12, electronic supplementary information), suggesting a significant conformational restriction must be responsible for the reduced decay of the excited state energy of the conformer.

3. Conclusion

We have designed and developed a novel long-wavelength emitting charge transfer probe. Our design is based on a donor- π - π -acceptor fluorophoric framework that can undergo deprotonation at physiological pH to produce a new fluorochrome.

The new fluorochrome displayed turn-on response toward HSA, both in the red and NIR-I region of the spectrum. It selectively responded to HSA over other common proteins and enzymes, including homologue BSA. Based on concentration dependent titration experiments the limit of detections were calculated and found to be 10 mg/L and 20 mg/L in the red and NIR-I window, respectively. The fluorescence enhancement of the probe was attributed to the minimization of the torsional modes of deactivation of the dimethine-bridge. The selective sensing mechanism was investigated by the displacement assays and molecular docking, and it was ascribed to a strong supramolecular complex of the probe at a specific site of HSA.

The dual emission window and the selective turn-on response toward HSA make **1** a practically viable probe for biological applications [43]. Moreover, the strategy of generating a stronger phenolate donor from its latent form provides a convenient route to produce background free turn-on probes for various biological applications. The introduction of various substituents on the benzene ring to manipulate the intramolecular charge transfer to extend the absorption and emission wavelengths appears to be a viable approach. Such fluorophore should be accessible synthetically from condensation reaction between an aldehyde precursor and a reactive acceptor.

CRedit authorship contribution statement

Rajib Choudhury: Conceptualization, Methodology, Resources, Writing - original draft, Supervision, Project administration, Funding acquisition, Investigation, Validation. **Benjamin Quattlebaum:** Investigation, Formal analysis. **Charles Conkin:** Investigation, Formal analysis. **Siddhi Rajeshbhai Patel:** Investigation, Visualization. **Kallie Mendenhall:** Investigation.

Declaration of competing interest

The authors declare that they have no known competing financial interests or personal relationships that could have appeared to influence the work reported in this paper.

Acknowledgements

This publication was made possible by the Arkansas INBRE program, supported by a grant from the National Institute of General Medical Sciences (NIGMS), and P20 GM103429 from the National Institutes of Health. We wish to thank Dr. Anindya Ghosh at University of Arkansas, Little Rock, for collecting the ^1H and ^{13}C NMR spectra.

Appendix A. Supplementary data

Details of the synthesis of the probes, ^1H and ^{13}C NMR spectra, photostability study under visible light, details of molecular dockings, titration experiments, and additional spectra. This material is available online via www.elsevier.com. Supplementary data to this article can be found online at doi: [10.1016/j.saa.2020.118305](https://doi.org/10.1016/j.saa.2020.118305).

References

- [1] G.J. Quinlan, G.S. Martin, T.W. Evans, *Hepatology* 41 (2005) 1211–1219.
- [2] T. Peters, *All About Albumin: Biochemistry, Genetics, and Medical Applications*, Academic Press Inc, San Diego, USA, 1996.
- [3] B.T. Dumas, T. Peters, *Clin. Chim. Acta* 258 (1997) 3–20.
- [4] S. Arques, P. Ambrosi, *J. Card. Failure* 17 (2011) 451–458.
- [5] K. Hoogenberg, W.J. Sluiter, R.P. Dullaart, *Acta Endocrinol.* 129 (1993) 151–157.
- [6] R. Amin, B. Widmer, A.T. Prevost, P. Schwarze, J. Coope, J. Edge, L. Marcovecchio, A. Neil, R.N. Dalton, D.B. Dunger, *Br. Med. J.* 336 (2008) 697–701.
- [7] H. Thakkar, D.J. Newman, F. Holownia, C.L. Davey, C.C. Wang, J. Lloyd, A.R. Craig, C.P. Price, *Clin. Chem.* 43 (1997) 109–113.
- [8] Z.Z. Huang, H.N. Wang, W.S. Yang, *Appl. Mater. Interface* 7 (2015) 8990–8999.
- [9] H.X. Sun, J.F. Xiang, X.F. Zhang, H.B. Chen, Q.F. Yang, Q. Li, A.J. Guan, Q. Shang, Y.L. Tang, G.Z. Xu, *Analyst* 139 (2014) 581–584.
- [10] R.E. Wang, L. Tian, Y. Chang, *J. Pharm. Biomed. Anal.* 63 (2012) 165–169.
- [11] D. Caballero, E. Martinez, J. Bausells, A. Errachid, J. Samitier, *Anal. Chim. Acta* 720 (2012) 43–48.
- [12] M.C. Tu, Y.Z. Chang, Y.T. Kang, H.Y. Chang, P. Chang, T.R. Yew, *Biosens. Bioelectron.* 34 (2012) 286–290.
- [13] Z. Luo, B. Liu, K. Zhu, Y. Huang, C. Pan, B. Wang, L. Wang, *Dyes Pigm.* 152 (2018) 60–66.
- [14] R. Singh, F.W. Crow, N. Babic, W.H. Lutz, J.C. Lieske, T.S. Larson, R.A. Kumar, *Clin. Chem.* 53 (2007) 540–542.
- [15] Y. Ermolenko, A. Anshakova, N. Osipova, M. Kamentsev, O. Maksimenko, V. Balabanyan, S. Gelperina, *J. Pharmacol. Toxicol. Methods* 85 (2017) 55–60.
- [16] X.D. Zeng, M.S. Ma, B.C. Zhu, L.A. Zhu, *Anal. Sci.* 32 (2016) 1291–1294.
- [17] K. Rajasekhar, J.A. Chaithra, T. Govindaraju, *Org. Biomol. Chem.* 15 (2017) 1584–1588.
- [18] S. Samanta, S. Halder, G. Das, *Anal. Chem.* 90 (2018) 7561–7568.
- [19] S.I. Reja, I.A. Khan, V. Bhalla, M. Kumar, *Chem. Commun.* 52 (2016) 1182–1185.
- [20] R. Choudhury, H.E. Parker, C.M. Cendejas, K.L. Mendenhall, *Tet. Lett.* 59 (2018) 3020–3025.
- [21] R. Choudhury, S.R. Patel, H.R. Lykins, *The Chemist* 91 (2018) 27–32.
- [22] R. Choudhury, S.R. Patel, A. Ghosh, *J. Photochem. Photobiol. A* 376 (2019) 100–107.
- [23] G. Chakraborty, A.K. Ray, P.K. Singh, H. Pal, *Chem. Commun.* 54 (2018) 8383–8386.
- [24] Q. Jin, L. Feng, S. Zhang, D. Wang, F. Wang, Y. Zhang, J. Cui, W. Guo, G. Ge, L. Yang, *Anal. Chem.* 89 (2017) 9884–9891.
- [25] Q. Sun, W. Wang, Z. Chen, Y. Yao, W. Zhang, L. Duan, J. Qian, *Chem. Commun.* 53 (2017) 6432–6435.
- [26] S. Sakamoto, T. Komatsu, T. Ueno, K. Hanaoka, Y. Urano, *Bioorg. Med. Chem. Lett.* 27 (2017) 3464–3467.
- [27] C. Staudinger, S.M. Borisov, *Methods Appl. Fluoresc.* (2015) 42005.
- [28] W.E. Moerner, R.J. Tweig, D.W. Kline, M. He, U.S. Patent 20070134737A1, 2007.
- [29] Z.R. Grabowski, K. Rotkiewicz, *Chem. Rev.* 103 (2003) 3899–4031.
- [30] P.D.E. Pretsch, T. Clerc, J. Seibl, W. Simon, *Spectral Data for Structure Determination of Organic Compounds*, Springer-Verlag, Heidelberg, 1989.
- [31] F.A.S. Chipen, A. Mishra, G. Krishnamoorthy, *Phys. Chem. Chem. Phys.* 14 (2012) 8775–8790.
- [32] M. Ipyu, C. Billon, G. Micouin, J. Samarut, C. Andraud, Y. Bretonniere, *Org. Biomol. Chem.* 12 (2014) 3641–3648.
- [33] A. Maliakal, G. Lem, N.J. Turro, R. Ravichandran, J.C. Suhadolnik, A.D. DeBellis, M.G. Wood, J. Lau, *J. Phys. Chem. A* 106 (2002) 7680–7689.
- [34] B. Wandelt, P. Turkewitsh, B.R. Stranix, G.D. Darling, *Faraday Trans.* 91 (1995) 4199–4205.
- [35] A.S. Tatikolov, S.M.B. Costa, *Biophys. Chem.* 107 (2004) 33–49.
- [36] G.L. Long, J.D. Winefordner, *Anal. Chem.* 55 (1983) 712–724.
- [37] N.E. Basken, G.J. Mathias, M.A. Green, *J. Pharm. Sci.* 98 (2009) 2170–2179.
- [38] I. Petitpas, A.A. Bhattacharya, S. Twine, M. East, S. Curry, *J. Biol. Chem.* 276 (2001) 22804–22809.
- [39] L. Karami, E. Tazikeh-Lemeski, A.A. Saboury, *Phys. Chem. Res.* 5 (2017) 483–496.
- [40] O. Trott, A.J. Olson, *J. Comput. Chem.* 31 (2009) 455–461.
- [41] H.A. Benesi, J.H. Hildebrand, *J. Am. Chem. Soc.* 71 (1949) 2703–2707.
- [42] Y. Akdogan, J. Reichenwallner, D. Hinderberger, *PLoS One* 7 (e45681) (2012) 1–9.
- [43] R. Tian, et al., *Sci. Adv.* 5 (2019) 1–11.